Accurately Measuring Slowly Propagating Flame Speeds: Application to Ammonia/Air Flames

Joel Mathew[a], Justin K. Tavares[a], Jagannath Jayachandran[a*]

[a]*Aerospace Engineering, Worcester Polytechnic Institute, 100 Institute Rd, Worcester, MA 01609, USA*

Abstract:
Environmental concerns have driven the development of alternative fuels and refrigerant working fluids with low global warming potential. Ammonia (NH_3) is a potential zero-carbon fuel, while hydrofluorocarbons (HFCs) like R-32 and R-1234yf are being adopted as refrigerants. When mixed with air, these compounds can sustain slowly propagating flames with laminar flame speeds less than 10 cm/s. Unlike typical hydrocarbon-fueled flames, these slow flames are influenced by buoyancy-induced flow and radiation heat loss. In this study, we experimentally investigate the flame speeds of NH_3/air mixtures using the constant-pressure spherically expanding flame method, while circumventing gravity-induced natural convection, and account for radiation-induced inward flow. To mitigate buoyant convection, a low-cost drop tower was built and used to study slow spherically expanding flames in free fall. A computational model (SRADIF) is utilized that combines thermodynamic equilibrium and finite rate optically thin limit radiation heat loss calculations to estimate the inward flow. The developed methodology is utilized to investigate slowly propagating NH_3/air flames over a range of equivalence ratios. A systematic approach was undertaken to understand and quantify the errors that could arise when deriving the laminar flame speed. It was found that attempting to study slowly propagating flames in a static configuration, as opposed to in free fall, results in large differences in flame dynamics and subsequently all derived quantities. It is necessary to study slowly propagating flames in free-fall. Additionally, using experimental data that has not been corrected for radiation-induced flow leads to large errors in all derived quantities. Furthermore, direct comparisons of experimental measurements and detailed flame simulations are found to be necessary to determine if existing extrapolation approaches are applicable to these slowly propagating flames, which are challenging to study.

Keywords: Laminar Flame Speed; Sustainable Fuel; Ammonia combustion; Microgravity

* Corresponding author.
E-mail address: jjayachandran@wpi.edu

Novelty and Significance Statement:
In this study, a novel methodology to accurately quantify slowly propagating flame speeds is presented. It consists of a combined, experimental approach to circumvent gravity-induced natural convection and a computational approach that accurately accounts for radiation-induced inward flow. This constitutes the first study that systematically investigates the errors that can arise while deriving the laminar flame speeds of slowly propagating flames from expanding rate measurements. Furthermore, accurate measurements are performed for the first time for NH_3/air flames.

Author Contributions:
JM: Experimental; Validation; Investigation; Methodology; Data Analysis; Writing
JT: Software; Validation; Investigation; Data Analysis; Writing
JJ: Conceptualization; Software; Investigation; Methodology; Data Analysis; Writing; Resources; Supervision

1. Introduction

Environmental concerns have motivated the development of alternate fuels and refrigerant working fluids that have low global warming potential. Ammonia (NH_3) is a candidate zero-carbon fuel and hydrofluorocarbons (HFCs) such as R-32, R-1234yf, etc. are being adopted as refrigerants. Upon mixing with air, these compounds can sustain flames that are slowly propagating i.e., with laminar flame speeds less than 10 cm/s. These flames are referred to as *slow* as they are affected by gravity (buoyancy-induced flow) [1, 2] and radiation heat loss [3], in contrast to typical hydrocarbon-fueled flames. Quantifying their reactivity is key to assessing the explosion risk associated with the storage, transportation, and utilization of these compounds.

The laminar flame speed (S_u^0) is a fundamental combustion property of a combustible mixture [4-6]. S_u^0 measurements are useful for assessing the reactivity of fuels and working fluids. More importantly, they serve as validation targets to constrain the uncertainty of chemical kinetic models [7]. Constrained kinetic models are invaluable. In the case of HFCs, they can estimate the reactivity of mixtures of HFCs, thereby enabling the development of refrigerant blends with favorable flammability, sustainability, and performance characteristics [8]. Kinetic models can also be used in conjunction with fluid models to assess fire and explosion risk associated with leakage followed by accidental ignition of these compounds [6].

A survey of literature reveals that the vast majority of measurements for NH_3/air and HFC/air flames have been made using the spherically expanding flame (SEF) configuration. The reason is that NH_3, and the products of HFC combustion, hydrogen fluoride and carbonyl fluoride, are toxic. The counterflow and heat flux approaches need a continuous flow of reactants. In contrast, the SEF approach utilizes only a small amount of reactants, resulting in a correspondingly small quantity of products, which are contained in a sealed combustion chamber, and can be exhausted safely. Additionally, the well-defined stretch rate and short experimental time scales (which make the configuration more amenable to be studied in a drop tower as discussed later) make this configuration attractive [6]. Consequently, we utilize the constant pressure SEF (CONP-SEF) approach for measuring S_u^0. The CONP approach (as opposed to the constant volume approach (CONV-SEF) [6] is preferred as optical access allows for tracking the onset of flame-front instabilities, and the distortion of flames due to natural convection. All subsequent discussions concern CONP-SEFs unless specifically mentioned.

Two aspects make accurate measurements of slowly propagating flame speeds challenging: buoyancy-induced flow and radiation heat loss. Although ubiquitous, they affect flame propagation only when the relevant time scale becomes comparable to, or less than, the characteristic time scale of flame propagation [2].

Gravitational forces induce flow due to the significant difference in density between the hot burned and cold unburned gases [1]. For SEFs, this buoyant convection results in the flame deforming into a dimpled, oblate-ellipsoid [1, 9]. The extent to which a flame is deformed can be estimated using the Richardson number (***Ri***), which compares the characteristic time scale of flame propagation to the characteristic time scale of buoyant convection [1, 9].

$$Ri = \frac{(\rho_u - \rho_b)}{\rho_u} \frac{gR_f}{\left(\dot{R}_f\right)^2}$$

Here ρ_u and ρ_b are the unburned and (adiabatic) burned gas densities, respectively, g is the gravitational acceleration, R_f is the flame radius and $\dot{R}_f$ is the flame expansion rate in the laboratory frame of reference. Using direct numerical simulations (DNS), Berger et al. [9] showed that SEFs with Ri approaching or greater than unity become significantly distorted, and as a result, the extracted S_u^0 could be erroneous. Since, R_f is ill-defined for a buoyant flame, they evaluated a variety of methods to extract flame speed information from the distorted flames to determine if S_u^0 can be accurately derived [9]. The only relatively accurate method they found is the surface-averaged displacement speed which uses the

geometrical features of the buoyant flame. However, the derived expression is contingent on the assumption that the average burned gas density does not change with time [9]. However, this is not applicable for slowly propagating flames, which are known to have significant radiation heat loss.

For a slowly expanding flame with S_u^0 ~ 8 cm/s, R_f = 3 cm, and ρ_u/ρ_b ~ 7, Ri ~ 1. Whereas for S_u^0 ~ 30 cm/s with everything else being similar, Ri ~ 0.04. Based on this analysis, it is evident that slowly propagating spherical flames (such as NH_3/air, R-32/air, etc.) will be deformed by buoyancy, making measurements of S_u^0 challenging.

Buoyancy-induced flow can be minimized by studying SEFs in *free fall* (as opposed to in the typical *static* configuration). However, the inaccessibility of microgravity combustion facilities (e.g., parabolic flight vehicles, drop towers, low earth orbit space vehicles) has restricted free fall experimental investigations of slow flames to a handful of datasets [10-17]. Measurements have been performed for HFC/air [11, 17], and NH_3/air [12]. However, these measurements do not account for the effects of radiation heat loss. Ronney [12] examined the role of chemical kinetics and transport properties of near-limit flames in free fall. He found that NH_3/air flames display near-limit behavior (i.e., ignition limits, extinguishment limits, and near-limit burning velocities) similar to hydrocarbon/air mixtures that have similar effective Lewis numbers or transport properties [12]. Hesse et al. [11] measured the S_u^0 for nitrogen-diluted R-32/air flames in free fall. They found that accurate measurements for these flames are greatly hindered by ignition effects [11]. Specifically, they observed that ignition effects lasted beyond flame radii of 1 cm, which restricts the available data range to derive S_u^0 [11]. This is significant considering that the useable R_f range for their combustion chamber is from 1 cm to 2 cm [11]. This is attributed to the increased energy required for ignition due to conduction heat loss to the electrodes, which is not present in static experiments as the flame detaches rapidly from the electrodes [11]. Ronney [12] also found ignition challenging and argues that for large Lewis number mixtures, he observed ignition limits as opposed to flammability limits. Takizawa et al. [17] found good agreement between static and free fall experiments for R-32/air flames using the CONV-SEF approach. However, aside from Hesse et al. [11], these free fall measurements do not account for stretch effects which can lead to large errors in S_u^0.

Radiation heat loss effects in strongly burning and near-limit hydrocarbon/air flames have been extensively studied in the literature [3, 18-21]. Recently, the study of radiative effects was extended to slowly propagating HFC/air and NH_3/air flames [22-28]. Radiation heat loss results in a reduction of the maximum flame temperature, and consequently the overall reactivity and S_u^0 [3, 19, 21, 29]. This effect is henceforth referred to as flame zone losses.

For SEFs, in addition to flame zone losses, cooling of the burned gas due to radiation heat loss induces an inward flow (radiation-induced inward flow, u_b) directed towards the center of the flame [3, 20, 21, 28]. Not accounting for this induced flow while interpreting expanding rate measurements of slow flames can result in large errors in the derived S_u^0 values [3, 20, 21]. Yu et al. [30] developed a correlation for correcting SEF data (mixtures of H_2, CO, and hydrocarbons with air) to retrieve the *adiabatic* S_u^0. This correlation, which was obtained from simulations performed for an extensive range of mixture thermodynamic conditions, subtracts both the effects of radiation-induced flow and flame zone losses. Faghih et al. [27] developed a similar correlation for slow NH_3/air flames. Despite being easy to implement, the accuracy of the correlation depends inherently on the accuracy of the kinetic model used. Specifically, the cooling time which determines the extent of heat loss, and the sensitivity of burning rate to changes in adiabatic flame temperature (T_{ad}) which is required to estimate flame zone losses, are both dependent on reactivity and hence the kinetic model utilized. And, since kinetic models for NH_3 and HFC combustion are in their early stages of development (compared to hydrocarbons) and have large uncertainties, it is not desirable to utilize these correlations for such flames [28].

Santner et al. [21] developed an analytical model to estimate u_b for hydrocarbon/oxidizer SEFs at high pressures. Hesse et al. [24] utilized this model to interpret and correct R-32/air SEF data at elevated initial unburned gas temperatures (T_us) and pressures (Ps). However, as noted by Santner et al. [21], the analytical model becomes less accurate for very low flame speeds due to large reductions in flame temperature. Additionally, the model is best suited for flames that are thermo-diffusionally neutral, such

that the propagation speed is only a weak function of R_f. Tavares et al. [28] recently showed that applying Santner et al.'s model to slowly propagating R-32/air SEFs at normal T_u and P results in errors of up to 70% when estimating u_b. Tavares et al. [28] also introduced a computational model, SRADIF, which utilizes chemical equilibrium and radiative cooling in the optically thin limit (OTL) model to estimate the burned gas state and inward flow. This model was shown to accurately estimate the inward flow for R-32/air SEFs by relaxing a couple of key assumptions made in the analytical model: a) SRADIF allows for burned gas composition to change with cooling, which accurately captures changes in the extent of burned gas species (CO_2 and H_2O) dissociation, and b) SRADIF accounts for variation in thermodynamic and radiative properties (Planck mean absorption coefficient (κ_p)) with burned gas cooling. SRADIF (and the Santner et al. model [21]) uses experimental data to determine the timescale of radiative cooling, hence not requiring a kinetic model to estimate u_b.

Given the challenges with accurately measuring S_u^0s of slow flames, the purpose of this study is to develop a combined experimental and computational methodology that addresses the aforementioned issues presented by buoyancy-induced flow and radiation heat loss. A low-cost drop tower with a free fall time of 0.5s and a short turnaround time is developed and utilized to experimentally investigate spherical slowly propagating flames with a minimal influence of buoyant convection. The SRADIF model is utilized to account for the effect of radiation-induced flow, and accurately interpret the experimental results. The methodology is first applied to measure S_u^0 of a slowly propagating flame fueled by the most studied hydrocarbon, a CH_4/air flame at an equivalence ratio, ϕ = 0.6, P = 2 atm and T_u = 300 K. After demonstrating the ability of the adopted approach to accurately measure S_u^0s of slowly propagating flames, S_u^0s of NH_3/air flames at P = 1 atm and T_u = 300 K are measured over a range of ϕ. This study constitutes the first study, to the authors' knowledge, that circumvents buoyancy-induced flow and accurately accounts for radiation heat loss effects, and systematically investigates the errors that can arise while deriving S_u^0s of slowly propagating flames. The paper is organized as follows. Section 2 presents an overview of existing NH_3-fueled flame measurements. Section 3 details the experimental (3.1) and computational methodologies (3.2). This is followed by results and discussion for CH_4/air and NH_3/air mixtures in Sec. 4, and conclusions in Sec. 5.

2. Overview of NH_3-fueled flame studies

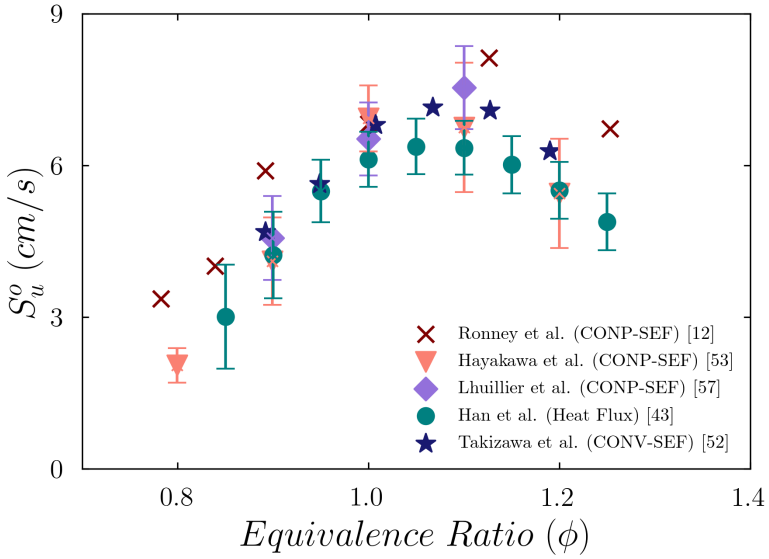

Figure 1: Select S_u^0 measurements of NH_3/air mixtures as a function of equivalence ratio (ϕ).

Ammonia combustion has garnered attention in recent years as a zero-carbon fuel and as a viable means of energy storage. The merits and drawbacks of NH_3 combustion are covered extensively in the following review papers: [31-35]. Flame chemistry of NH_3 is also relevant in the combustion of energetic materials like ammonium perchlorate and ammonium dinitramide, where it is formed as an intermediate species [36, 37]. Accurate measurements of NH_3/air flame properties are key to developing accurate chemical kinetic models not only for NH_3 combustion but also for the combustion of energetic materials.

The experimental challenges associated with studying NH_3/air combustion and the challenges of using pure NH_3 as a fuel due to its low reactivity have led researchers to investigate NH_3/H_2/air (a list of NH_3/H_2/air measurements is compiled in [38]) and NH_3/CH_4/air mixtures [39-44]. Han et al. [43] experimentally investigated the flame speeds of these blends and found that although the models (GRI-Mech 3.0 [45], Okafor et al. [46], San Diego [47]) they studied predicted the S_u^0s of CH_4/air and H_2/air mixtures well, they performed poorly when predicting the reactivity of NH_3/fuel/air blends. This is largely a result of the inaccurate rate constants of the reactions involving species with nitrogen. Another study by Zhu et al. [38] showed that S_u^0 shows large sensitivity to abstraction reactions involving nitrogen species as they inhibit reactivity by competing for hydrogen radicals in NH_3/H_2/air mixtures. This is again shown in the modeling work by Otomo et al. [48] where the improvement of their model in predicting S_u^0s of NH_3/air and NH_3/H_2/air flames is largely attributed to the modifications of reactions of nitrogen species. While these blends enhance reactivity and thereby facilitate experimental measurements, they may not isolate the important reactions involving nitrogen species, which will become more prominent for flames fueled only by NH_3.

Several measurements of NH_3/air flame speeds have been made in literature [12, 40, 49-60]. The earlier measurements [49-51] do not account for stretch effects, buoyancy, and radiation heat loss aside from Ronney [12] who performed experiments using a drop tower but did not account for stretch effects. As seen in Fig. 1, Ronney's measurements that were obtained during free fall are different from other measurements, obtained for example using the static SEF configuration. All recent S_u^0 measurements, that account for flame stretch, use the SEF method aside from Han et al. who used the heat flux method [40, 52-60]. Aside from accounting for stretch effects no advancements have been made pertaining to the accuracy of measuring NH_3/air flame speeds. Regarding buoyant convection, authors have used a variety of methods to extract an equivalent radius from the buoyant NH_3/air flames. The methods include: half the maximum horizontal flame dimension [50], radius of a circle that equals the projected flame area [53, 58], etc. As described earlier and shown in Sec. 4, these heuristic approaches result in large errors in the magnitude of the measured S_u^0 [9]. To address radiation heat loss effects, which are prominent in NH_3/air flames, several authors have utilized the correlation developed by Yu et al. for hydrocarbon/air flames to account for the error in NH_3/air flame speed measurements [40, 56, 57, 60]. However, this error is incorporated into the uncertainty analysis and does not improve the accuracy of flame speed measurements. Although the measurements by Han et al. [43] are nearly stretch-free, it is not clear how the data are affected by buoyancy-induced flow and radiation heat loss. Their S_u^0 values, as seen in Fig. 1, agree with the data of Hayakawa et al. [53] who used the CONP-SEF approach and did not account for radiation heat loss or buoyancy-induced flow. Another feature evident in Fig. 1 is the large discrepancy between S_u^0 measurements, ~2 cm/s for S_u^0 ~ 6 cm/s. This amounts to a difference of 30% and can be attributed to the issues that were discussed earlier, and potentially the different extrapolation techniques utilized. No study to date has compared the direct experimental measurements (e.g., dR_f/dt) from NH_3/air flames to DNS results, and systematically evaluated if large errors can arise during the extrapolation process [61].

3. Approach

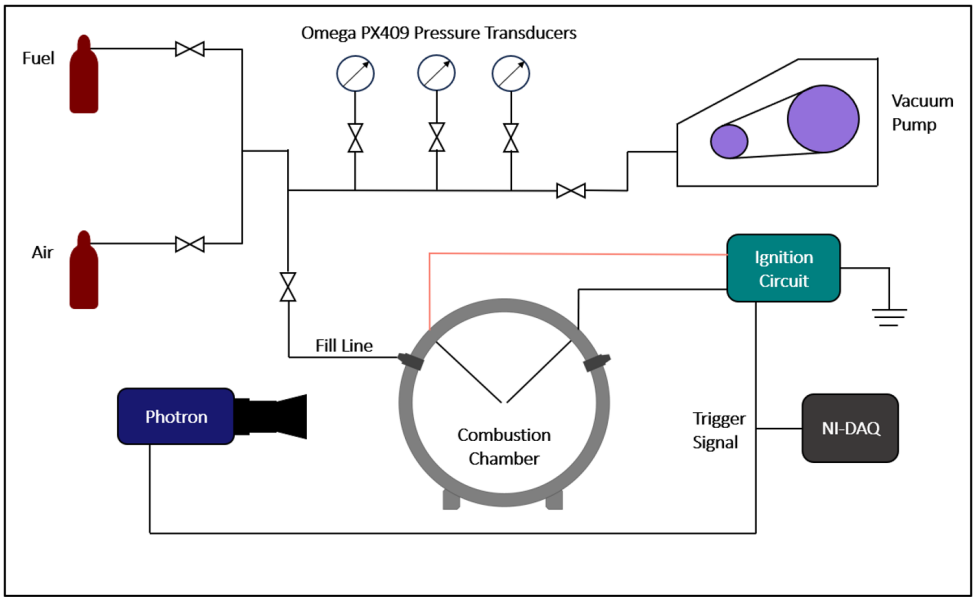

Figure 2: Schematic of the experimental facility.

Mixture	ϕ	P (atm)	Ri $(R_f = 3$ cm)	T_{ad} (K)	$R_{f,min}$ (cm)	$R_{f,max}$ (cm)
CH_4/air	0.6*	2	1.5	1642	2.1 ($\sim 30\delta_f$)	3.8
NH_3/air	0.8*	1	3.5	1864	1.7 ($\sim 7\delta_f$)	3.8
	0.9	1	1.8	1981	1.5 ($\sim 7\delta_f$)	3.8
	1.0*	1	1.1	2070	1.6 ($\sim 9\delta_f$)	3.8
	1.1	1	0.7	2029	1.8 ($\sim 11\delta_f$)	3.8
	1.2	1	0.8	1970	1.8 ($\sim 10\delta_f$)	3.8

Table 1: List of the mixtures studied and their relevant properties. $R_{f,min}$ and $R_{f,max}$ denote the upper and lower radius bounds used for interpretation, respectively. $R_{f,min}$ is also denoted as a multiple of the flame thickness, δ_f. (* indicates conditions for which both static and free-fall measurements were conducted)

3.1. Parameter Space

Static (only at select conditions) and free-fall measurements were performed for a CH_4/air flame at ϕ = 0.6, P = 1 atm and T_u = 300 K, and NH_3/air flames at P = 1 atm and T_u = 300 K over a range of ϕ, $0.8 \leq \phi \leq 1.2$; see Table 1. Attempts were made to ignite flames at ϕ = 0.7 and 1.3 for NH_3/air in free fall, however, these were unsuccessful. All cases included in this study were repeated twice to ensure consistency (see SM-H). Since this is the first study using this experimental facility, static experiments were also carried out for CH_4/air flames at P = 1 atm and T_u = 300 K to ensure that the adopted approach is capable of accurately measuring S_u^0s; details regarding these experiments and the results obtained can be

found in SM-D. The mixtures considered in this study are listed in Table 1. The experimental methods described below are identical for both the static and free-fall experiments, except the use of the drop tower (see Sec. 3.2.1) for the free-fall measurements.

3.2. Experimental Approach

All experiments are conducted in a 12.9 L, stainless steel cylindrical chamber with optical access at both ends; see Fig. 2. The internal diameter is 25.4 cm with an aspect ratio of unity. The combustion chamber is fitted with polycarbonate windows that are 1.8 cm thick with an optical diameter of 10.16 cm. The chamber is first vacuumed down to less than 40 Pa, and then filled with a mixture using the method of partial pressures. The equivalence ratio for NH_3/air cases is determined by the following stoichiometric reaction,

$$NH_3 + \frac{3}{4}(O_2 + 3.76N_2) \rightarrow \frac{3}{2}H_2O + \frac{13.28}{4}N_2$$

The fuel is filled first followed by the oxidizer, compressed air. The anhydrous NH_3 used has a purity of 99% and the compressed air is desiccated and filtered. Omega PX409-A5V series pressure transducers were used. The transducer with the appropriate full-scale pressure range was used to fill each gas to minimize the uncertainty in the equivalence ratio [62]. Ammonia adsorption, which has been discussed in prior studies, results in the pressure of NH_3 dropping over time which can result in a large deviation in equivalence ratio [43, 52, 59, 63]. This can be circumvented by waiting approximately an hour until the pressure drop is negligible [52, 59], which was verified with repeated tests.

The mixture was allowed to rest for at least 10 minutes before ignition to ensure the gas's quiescence. The chamber is equipped with two stainless steel electrodes (< 1 mm thickness, 1.5 mm spark gap), allowing for the central ignition of the mixture. A tunable capacitive discharge circuit allows for the spark energy to be tailored to minimize ignition effects on flame propagation. Due to the low reactivity of NH_3/air mixtures, substantially larger ignition energy is required in comparison to hydrocarbon/air mixtures. The ignition, drop, and recording are synchronized with a LabView program.

3.2.1. Drop Tower

For the free fall experiments, a lab-scale drop tower was designed and built to minimize buoyancy-induced flow distortions. The drop tower has dimensions of 1.16m x 1.16m x 2.65m and accommodates the chamber, a high-speed camera, and wiring. It consists of a platform on which the combustion chamber and camera are mounted. The platform is hoisted, aligned, and fixed in place by electromagnets that can be disengaged simultaneously for a precise release (see SM-A for images of the drop tower). The platform, which holds both the combustion chamber and camera, has dimensions of 0.4 m x 0.4 m x 0.01 m, weighs ~45 kg, and falls ~1.5 m when released by the electromagnets. A bed of foam cubes is used to decelerate the platform and bring it to rest while preventing any damage to the camera. The drop tower has a free fall time of ~0.5s. An in-house LabVIEW script simultaneously initiates recording, ignition, and the release of the combustion assembly. During free fall, a deviation of less than 2% from the acceleration due to gravity, predicted by theoretical analysis, is confirmed by optical measurements (see SM-A). This is sufficient to establish SEFs for the slowly propagating mixtures listed in Table 1.

3.2.2. Direct Imaging/Optical Calibration

The SEFs are directly imaged using a Photron FASTCAM Mini AX50 with a 50 mm focal length lens. Imaging was performed at 2000 fps with a 1024 × 1024 pixel imaging window. The use of direct imaging is necessary as the lab-scale drop tower cannot accommodate a schlieren/shadowgraph system. An optical calibration factor is required to convert the measured pixels to a length scale. The accuracy of this factor is of great importance as the error in S_u^0 is directly proportional to the error in the calibration factor. The advantage of schlieren/shadowgraph imaging is the use of parallel light which greatly facilitates optical calibration. Direct imaging of flame propagation at close distances is challenging due to the three-dimensional nature of the flame in combination with the light rays being not parallel [64]. Specifically, as the distance between the camera and the flame decreases, only a fraction of the hemisphere on the camera side is visible; the poles are not visible. Therefore, an error will result if a calibration factor that is developed using a planar calibration target is utilized to derive the radius of a sphere. To avoid this, an optical calibration technique was developed by imaging high-tolerance aluminum cylinders at various radii (0.635 cm – 3.81 cm) at a distance that was utilized for the experiments as well. Cylinders were chosen as spherical optical targets are prohibitively expensive to procure with dimensional tolerances small enough for calibration purposes. The cylinders provide a similar projection onto the camera sensor as a sphere, in one direction. More details of the procedure are provided in SM-C. The optical calibration results in a correlation that converts the imaged radii in pixels to length in cm. For the current study, the calibration factor is about 7 pixels/mm (does not change with the size of the object in the relevant range of radii), which is sufficient to resolve the flames considered.

The high-speed videos are post-processed using an in-house Python code to extract the radius of the flame. The images are minimally preprocessed using a Gaussian blur to smooth aberrant pixel noise. A numerical gradient of the image yields a set of points; a convex hull of these points yields the outer flame surface. A circle is fit to this set of points using the single-value-decomposition-based Taubin circle fit [65]. The aforementioned correlation is applied to convert the radii in pixels to flame radius, R_f, in cm. For buoyant, static flames, R_f is ill-defined as the flame is not spherical. A typical approach utilized in previous studies [12, 50, 55] is to track the maximal horizontal length of the flame and use half of this value as R_f. This method is also used for the static cases in this study to compare with the flame speeds obtained from free fall experiments at similar conditions denoted in Table 1. The method used to determine flame radius can have a large effect on the post-processed flame behavior. As Berger et al. [9] showed in their DNS study, flame stretch for buoyant flames varies with time along the flame front. This means that the point on the flame tracked by the maximal horizontal length method does not have the same flame stretch as the one obtained in free fall [9], and consequently, does not evolve in the same way; see Sec. 4 for more details.
A local second-order fit is applied to the R_f vs. time data to calculate the derivative, dR_f/dt. However, as stated earlier, this dR_f/dt results from a combination of the stretched, burned flame speed, S_b, and the radiation-induced inward gas velocity, u_b. To extract S_b, Eq. 1 [3] is used with u_b estimated using SRADIF (see Sec. 3.3.2). With the S_b and K (Eq. 2 [66]), an extrapolation must be used to compute the unstretched, burned flame speed S_b^0. Both linear (Eq. 3 [67]) and nonlinear extrapolation models (Eq. 4 [68, 69]) were applied to the inward-flow-corrected S_b vs. K results to obtain estimates for the unstretched, burned flame speed S_b^0 at zero K. The ranges of R_f for extrapolation are listed in Table 1. The upper bound ($R_{f,max}$) is chosen as 4 cm (30% of the chamber radius) to avoid confinement and pressure rise effects [70, 71]. The lower bound ($R_{f,min}$) is chosen in a way to avoid ignition-affected data. It has been shown in previous studies that ignition effects dissipate as the flame propagates about 5-10 flame thicknesses (δ_f) [72-74]. Based on this and the trends depicted by the acquired data, we chose $R_{f,min}$ to be at least $7\delta_f$ (calculated using the respective kinetic models). This is further discussed in Sec. 4.2.

The density ratio ρ_u/ρ_b of the adiabatic case (i.e., ρ_b computed assuming equilibrium conditions) was then used to convert S_b^0 to S_u^0 through mass continuity [28].

$$S_b = \frac{dR_f}{dt} - u_b \tag{1}$$

$$K = \frac{2}{R_f}\frac{dR_f}{dt} \tag{2}$$

$$S_b = S_b^0 - L_b K \tag{3}$$

$$\left(\frac{S_b}{S_b^0}\right)^2 ln\left(\frac{S_b}{S_b^0}\right)^2 = -\frac{2L_b K}{S_b^0} \tag{4}$$

An uncertainty analysis was performed following a method similar to that developed by Xiouris et al. [62]. Error bars in results depict the combined uncertainty, $\pm\sigma$, of the mixture preparation, data acquisition, and data processing steps. For the sake of clarity, the uncertainty bands will only be included in the S_u^0 and not in the dR_f/dt and S_b plots; however, the data and σs are included in SM-B. For more details regarding the uncertainty analysis, the reader is referred to SM-B.

3.3. Computational Approach

3.3.1. Planar and spherical flames

Planar, 1-D, steady, freely propagating flame simulations were performed using the free flame module of Cantera [75] including the effects of radiation heat loss. In addition, 1-D SEF DNS at constant pressure were performed using the reacting flow code SLTORC. Details regarding the ability of SLTORC to accurately simulate SEFs can be found in Tavares et al. [28]. SEFs are initialized by a kernel of hot burned gas, and a hyperbolic tangent profile is utilized to transition smoothly between the burned and unburned gas states. The ignition energy is controlled through parameters specifying the initial kernel radius and temperature, which were chosen so that ignition-related effects would be minimized, enabling quasi-steady propagation to be reached at radii relevant to constant-pressure SEF experiments. The time-evolution of R_f is determined using a user-specified isotherm. Convergence tests were conducted to determine proper values for parameters controlling grid refinement and time step size to allow for grid-independent solutions. For each mixture/case, DNS studies were performed assuming (1) adiabatic conditions, and (2) including radiation heat loss.

In the above planar and spherical flame simulations, radiation heat loss was modeled using the OTL assumption. The OTL model provides an analytical formulation for emission-dominated radiative heat loss flux ($\dot{q}_{rad}$) using Planck mean absorption coefficients (κ_p) of major radiating species. Radiation reabsorption is ignored in the OTL model, but this effect may need to be considered in future work for slowly propagating flames with relatively large optical thicknesses. Burgess et al. [76] have considered radiation reabsorption in spherical HFC/air flames, but limited their analysis to solely CO_2 reabsorption, as spectrally-resolved radiation properties are not available for HFC refrigerants [76]. Radiation reabsorption effects have been studied in planar NH_3/air flames considering the emission and reabsorption of NH_3 and H_2O [25] but have not been formally studied in spherical NH_3/air flames. However, radiation reabsorption has been shown to become more relevant at higher pressures and may need to be considered in high-pressure NH_3/air SEFs [25].

The FFCM-1 kinetic model [77] was used for CH_4/air flame simulations, and the kinetic models developed by Nakamura et al. [78], Stagni et al. [79], and Zhu et al. [38] were used to simulate NH_3/air flames. Comparisons with the other models, such as [38, 79], can be found in SM-G. For radiative CH_4/air flames, CO_2, H_2O, CO, and CH_4 were considered as major radiative species, while for radiative NH_3/air flames, H_2O, NH_3, NO, and N_2O were considered as major radiative species. The different values of κ_p for H_2O, CO_2, CO, and CH_4 were obtained from Barlow et al. [80], while the values of κ_p for NH_3, NO, and N_2O were obtained from Nakamura et al. [78]. The Cantera and SLTORC source codes were modified to include κ_p for radiative species relevant to CH_4/air and NH_3/air flames. The DNS results of SLTORC SEFs were subsequently post-processed to determine the evolution of dR_f/dt with K for both the adiabatic and radiative cases, as well as the evolution of R_f with t for the radiative case to be used in the SRADIF model.

3.3.2. Estimating radiation-induced flow

The SRADIF model was used to interpret experimental and DNS-generated R_f vs. t data, to correct for radiation-induced inward flow. Details related to the SRADIF model algorithm are briefly described below, and a detailed description can be found in Tavares et al. [28]. The SRADIF model discretizes a sufficiently large spherical gas volume into layers of thin spherical shells of equal width and combines thermodynamic equilibrium and finite rate OTL radiation heat loss calculations to estimate u_b. Spherical shells are iteratively combusted by performing thermodynamic calculations, using the equilibrium capabilities of Cantera [75], to estimate the gas state at the maximum flame temperature of the radiative flame. During each combusted shell iteration, the SRADIF model accounts for finite-rate radiation heat loss in previously burned gas shells using a radiative cooling time scale derived from R_f vs. t measurements. Temperature reductions in each burned gas shell are computed using the OTL radiation model accounting for select radiative species through the different values of κ_p. For each combusted shell iteration, the total shrinkage of burned gas shells due to radiative cooling (i.e., due to reductions in burned gas shell temperature) and the radiative cooling time scale are then used to compute u_b. Iterating through the combustion of all spherical shells provides the evolution of u_b with K, which can be subtracted from dR_f/dt to obtain S_b.

In this study, the thermodynamic data of the FFCM-1 [77] and Nakamura et al. [78] chemical models were used to compute gas state properties and equilibrium states for CH_4/air and NH_3/air cases, respectively. Additionally, the different values of κ_p are incorporated in the OTL radiation models of Cantera and SLTORC (as described in Sec. 3.3.1) were included in the SRADIF model. The number of spherical shells used by the SRADIF model was varied to ensure shell-independent solution convergence for u_b and S_b (~1000 shells).

S_bs derived using the abovementioned procedure are affected by flame zone (radiation heat) losses. Hence the S_u^0 subsequently derived from this S_b is not *adiabatic*. While Santner et al. [21] proposed a subsequent step to subtract the flame zone losses to obtain the adiabatic S_u^0, there are several drawbacks to using such a method. First, Santner et al. [21] make multiple assumptions to obtain a tractable analytical form for the flame zone loss correction. Second, the analytical form requires knowledge of the overall or global activation energy (sensitivity of changes in burning flux to changes in T_{ad}), often obtained utilizing detailed chemical kinetic models [28]. Since kinetic models for slowly propagating flames (NH_3/air, HFC/air, etc.) have large uncertainties, the corresponding flame zone loss corrections derived will also be highly uncertain. Therefore, for the purpose of testing kinetic models, it is of more utility to compare the flame-zone-heat-loss-affected S_b measurements to model predictions that are also affected by flame zone losses. Therefore, corrections for flame zone losses were not performed in this study.

4. Results and Discussion

4.1. Methane/air

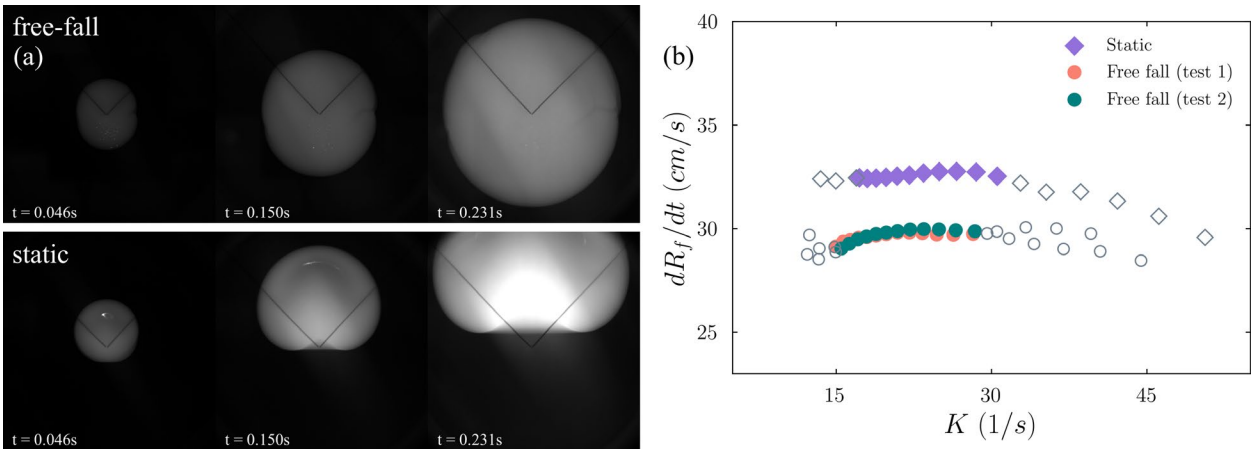

Figure 3: a) Static versus free fall temporal evolution for a CH_4/air flame (ϕ = 0.6, P = 2 atm, T_u = 300 K) b) Measured, static versus free fall (filled symbols denote data useable for extrapolation), dR_f/dt as a function of flame stretch for the same CH_4/air flame with data from two experimental trials shown for the free fall measurements.

As discussed in Sec. 1, we first study a slowly propagating CH_4/air flame at ϕ = 0.6, P = 2 atm, and T_u = 300 K. CH_4 is a well-studied hydrocarbon and hence a suitable candidate to first apply the experimental and interpretational approach detailed in Sec. 3. The flame evolution under static and free fall conditions are depicted in Fig. 3a. It is clear that under static conditions the flame undergoes significant distortion as well as upward displacement. However, under free fall conditions, the flame remains more or less spherical, as desired. The deviation from sphericity was also quantified and found to be minimal; more information about this can be found in SM-K. Figure 3b depicts the dR_f/dt values extracted from these experiments. The free-fall experiments show a high degree of repeatability with the mean, measured flame speeds for the consecutive free-fall runs differing by less than 0.5% in the region used for extrapolation. Note that for the static experiments, R_f is half the maximum horizontal diameter of the distorted flame, and K is calculated based on this radius. It is clear that the dR_f/dt vs. K behavior is different between the static and free fall measurements. The values extracted from the static case are larger than those from the free fall experiments, similar to the computational results of Berger et al. [9]. If an extrapolation (e.g., linear) is performed using these two sets of data to subtract the effects of stretch, the resulting flame speeds will differ by 14%. However, as discussed in Sec. 3.2.2 (Eqn. 1), S_b has to be derived from dR_f/dt, by correcting for the radiation-induced flow, before an extrapolation procedure can be applied.

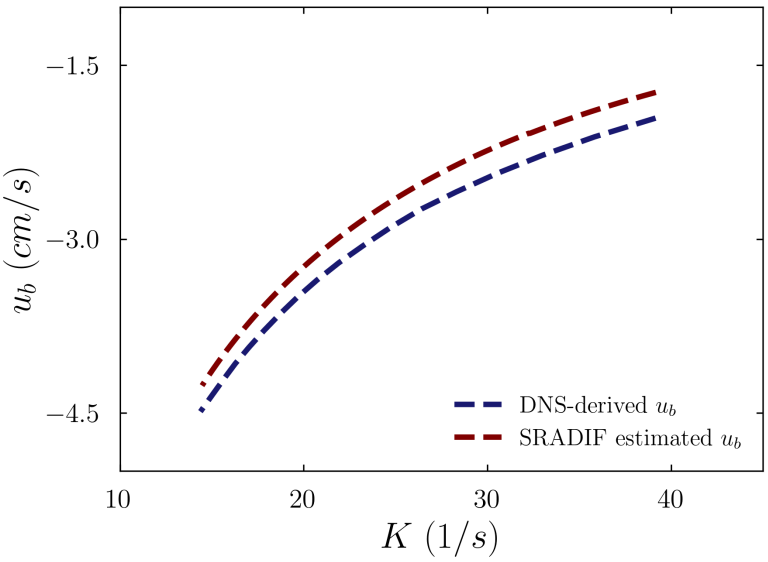

Figure 4: Comparison of DNS-derived and SRADIF-estimated u_bs for a CH_4/air flame at ϕ = 0.6, P = 2 atm, T_u = 300 K

We utilize SRADIF to estimate the radiation-induced flow, u_b. The accuracy of SRADIF depends on its ability to predict the burned gas state (temperature and species mole fractions) just downstream of the flame. Tavares et al. [28] showed that if the burned gas does not attain equilibrium (i.e., the state of the gas at the maximum flame temperature greatly differs from the equilibrium state), the burned gas temperature and species composition cannot be calculated using equilibrium thermodynamics and leads to large errors in the SRADIF-estimated u_b values. In a previous study by Tavares et al. [28], it was shown that SRADIF was able to accurately estimate u_b for R-32 flames. But the u_b values for R-1234yf/air SEFs had large errors, the reason being that the burned gas did not attain equilibrium as the heat loss resulted in the reacting gas getting frozen at a different metastable state; more details can be found in [28]. Therefore, it is important to test the accuracy of the SRADIF model before utilizing it for slowly propagating CH_4/air and NH_3/air flames considered in this study.

DNS was performed for the same spherically expanding CH_4/air flame at ϕ = 0.6, P = 2 atm, and T_u = 300 K including radiation heat loss. The full field results were utilized to calculate u_b using the methodology detailed in Tavares et al. [28]. They derived the inward gas velocity field induced by radiation heat loss $u_{rad}(r)$ as a function of radial distance r given by Eq. (5),

$$u_{rad}(r) = -\frac{1}{r^2}\int_0^r \frac{\dot{q}_{rad}}{\rho c_p T}\bar{r}^2 d\bar{r} \tag{5}$$

where $\dot{q}_{rad}$ is the volumetric radiative heat loss flux (calculated using the OTL radiation model), ρ is gas density, c_p is specific heat at constant pressure, T is temperature, and $\bar{r}$ is a radial integration variable. Subsequently, u_b is computed by taking the minimum of $u_{rad}(r)$, which occurs in the proximity of the flame zone. Values for u_b computed directly from DNS results are compared to u_b values estimated using SRADIF in Fig. 4. Note that, in order to estimate u_b, SRADIF takes as input, only R_f vs t from the DNS result and the unburned mixture condition. It is evident that SRADIF is able to accurately estimate u_b for the slowly propagating CH_4/air flame as the differences between the mean DNS-derived and SRADIF-estimated values were less than 10%. As S_b is obtained by subtracting u_b from dR_f/dt, which is numerically much larger (see Figs. 4 and 5), this amounts to less than 1% difference in SRADIF-corrected and DNS-corrected S_b values. In addition, it is also shown in SM-J that SRADIF performs significantly

better when compared to the Santner et al. model [21], which utilizes multiple simplifying assumptions as mentioned Sec. 1.

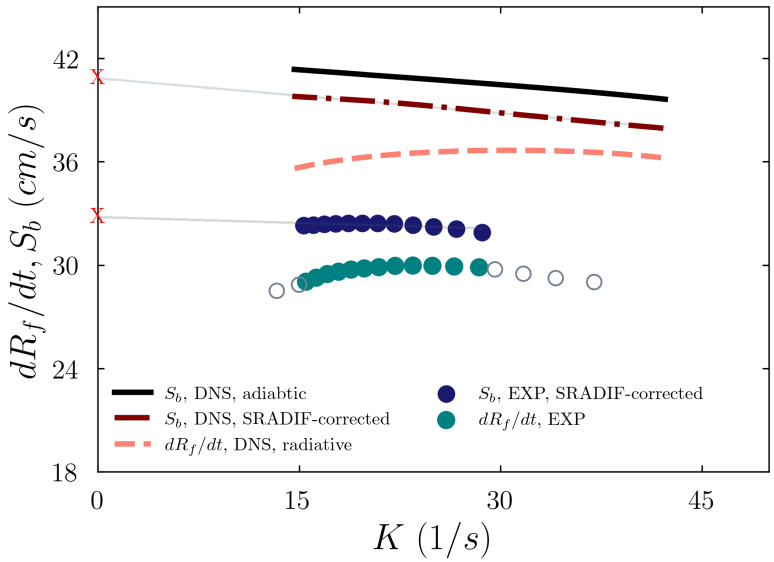

Figure 5: Spherical, CH_4/air flame with ϕ = 0.6, P = 2 atm, T_u = 300 K: SRADIF corrected experimentally measured data (filled symbols denote data useable for extrapolation) compared to adiabatic DNS computed dR_f/dt, OTL DNS computed dR_f/dt, and the SRADIF corrected OTL DNS curve.

Figure 5 depicts dR_f/dt and S_b, obtained from the free fall experiment as a function of K. S_b was derived by subtracting SRADIF-estimated u_b values from dR_f/dt. Also shown in the plot are dR_f/dt and S_b extracted from the DNS simulation result with radiation heat loss, and S_b (= dR_f/dt) from a DNS simulation assuming adiabaticity. Several observations can be made from these results. First, the slope of S_b vs. K is substantially different from dR_f/dt vs. K; the magnitudes are also different. Therefore, not correcting for radiation-induced flow can result in errors in S_u^0 of ~15%. Second, the DNS results indicate that the effect of radiation-induced flow on flame speed is significantly larger than the flame zone loss effect. This is evident through the larger difference between radiative S_b and radiative dR_f/dt compared to the difference between adiabatic S_b and radiative S_b. Third, although the slopes of experimentally derived dR_f/dt and S_b vs. K are similar to the corresponding DNS values, the linearly extrapolated values (Eqn. 3) differ by ~22%. This is also reflected in the extrapolated S_b^0, and density corrected S_u^0. It is worth examining if any of the assumptions that were utilized in data interpretation or modeling caused this large difference between the experiment and model prediction. The assumption that radiation reabsorption is negligible may not be entirely applicable under this condition. However, this does not explain the difference, as including reabsorption in the DNS calculations will only increase the value of simulated dR_f/dt, making the difference between data and simulation larger. The derived experimental S_u^0 is also compared to existing measurements at the same condition [81-83] in SM-E; these data were used to optimize and reduce the uncertainty of FFCM-1, the kinetic model used for the simulations. The discrepancies between our derived S_u^0 and existing data can be attributed to previous studies not accounting for the effects of buoyancy-induced flow and radiation heat loss. These results demonstrate the importance of accounting for buoyancy and radiation heat loss effects when interpreting slowly propagating flame data.

4.2. Ammonia/air

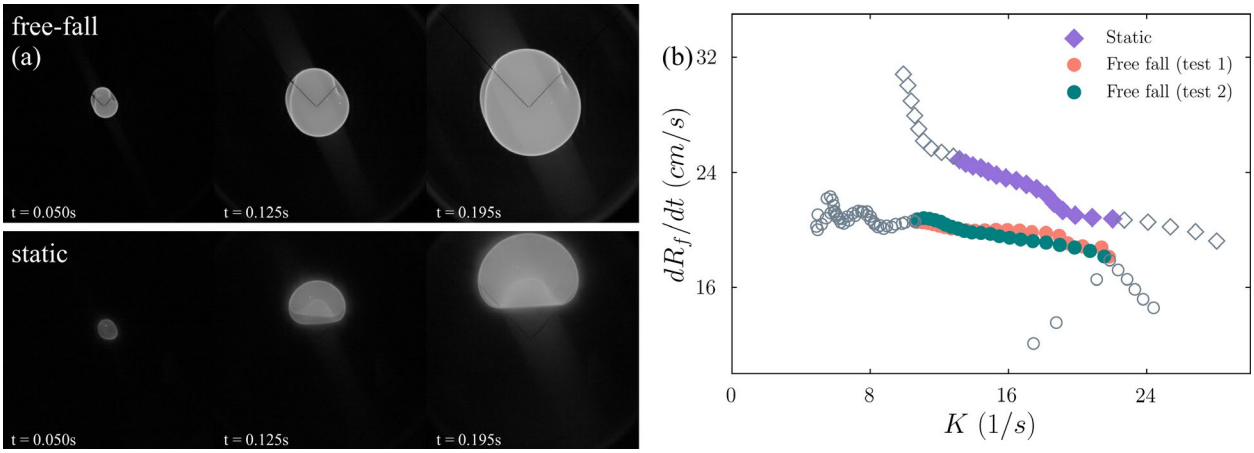

Figure 6: a) Static versus free fall temporal evolution for an NH_3/air flame (ϕ = 0.8, P = 1 atm, T_u = 300 K) b) Measured, static versus free fall (filled symbols denotes data useable for extrapolation), dR_f/dt as a function of flame stretch for an NH_3/air flame (ϕ = 0.8, P = 1 atm, T_u = 300 K)

NH_3/air SEFs at P = 1 atm, T_u = 300 K, and 0.8 ≤ ϕ ≤ 1.2 are studied in free fall. Static experiments were also performed for ϕ = 0.8 and ϕ = 1.0 to evaluate the errors that result if S_u^0s are derived from buoyancy-distorted flames instead of spherical flames obtained under free fall. Being the slowest flame with the largest *Ri* (see Table 1), the ϕ = 0.8 case is chosen for an in-depth analysis. Results for the ϕ = 1.0 case can found in SM-I. Figure 6a shows the evolution of the SEF under static and free-fall conditions. Figure 6b depicts the dR_f/dt values extracted from these `experiments. Consecutive free-fall runs for this case are shown in Fig. 6b to highlight the repeatability of the experimental methodology. It is observed in Fig. 6a that the morphology of the flames are significantly different. Under static conditions, the flame develops the distinct shape of a mushroom with the stem removed. The flow field that develops and causes this distinct shape is described in the DNS study by Berger et al. [9]. However, in free fall, the flame remains spherical, demonstrating the capability and precision of the low-cost drop tower to experimentally probe slowly propagating flames. The deviation from sphericity was also quantified and found to be minimal; more information about this can be found in SM-K. Additionally, as seen in Fig. 6b, it is clear that dR_f/dt vs. K behavior is markedly different between the static and free fall measurements. The same method described in Sec. 4.1 was used to extract the radius of the buoyant, non-spherical flame. The values extracted from the static case are larger than those from the free-fall experiments and a linear extrapolation of the static case within the usable data range would result in a 44% larger S_b^0 as a result of the large differences in slope! Also, note the substantial increase in dR_f/dt at large R_f (or small K). This was also observed in other measurements [40, 53] and DNS [9], and is most likely due to the flow field that develops during flame distortion.

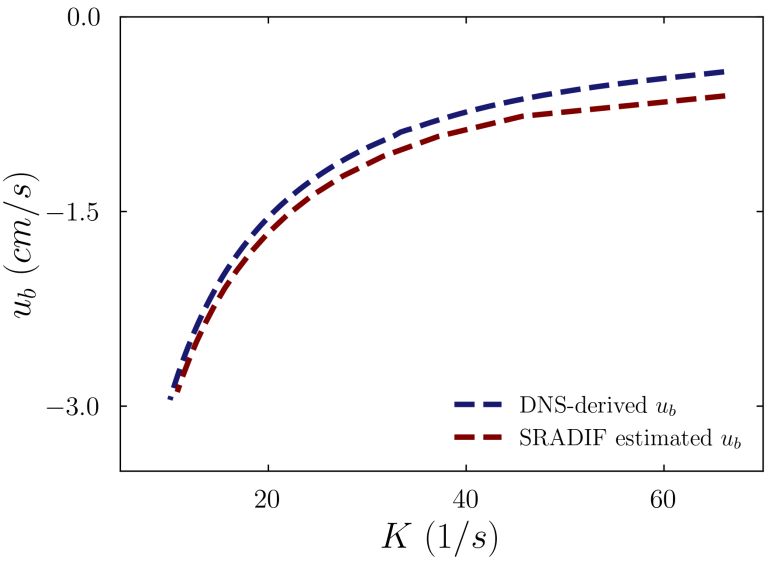

Figure 7: Comparison of DNS-derived and SRADIF-estimated u_bs for an NH_3/air flame at ϕ = 0.8, P = 1 atm, T_u = 300 K

DNS was performed for the same spherically expanding NH_3/air flame at ϕ = 0.8, P = 1 atm, T_u = 300 K including radiation heat loss. The full field results were utilized to calculate u_b [28]. These values are compared to u_b values estimated using SRADIF in Fig. 7. Clearly, SRADIF can accurately estimate u_b for the slowly propagating NH_3/air flame as the percent differences between DNS-derived and SRADIF-estimated values is ~5% which results in a 0.6% difference in the corresponding S_b. This was found to be the case for other ϕs as well.

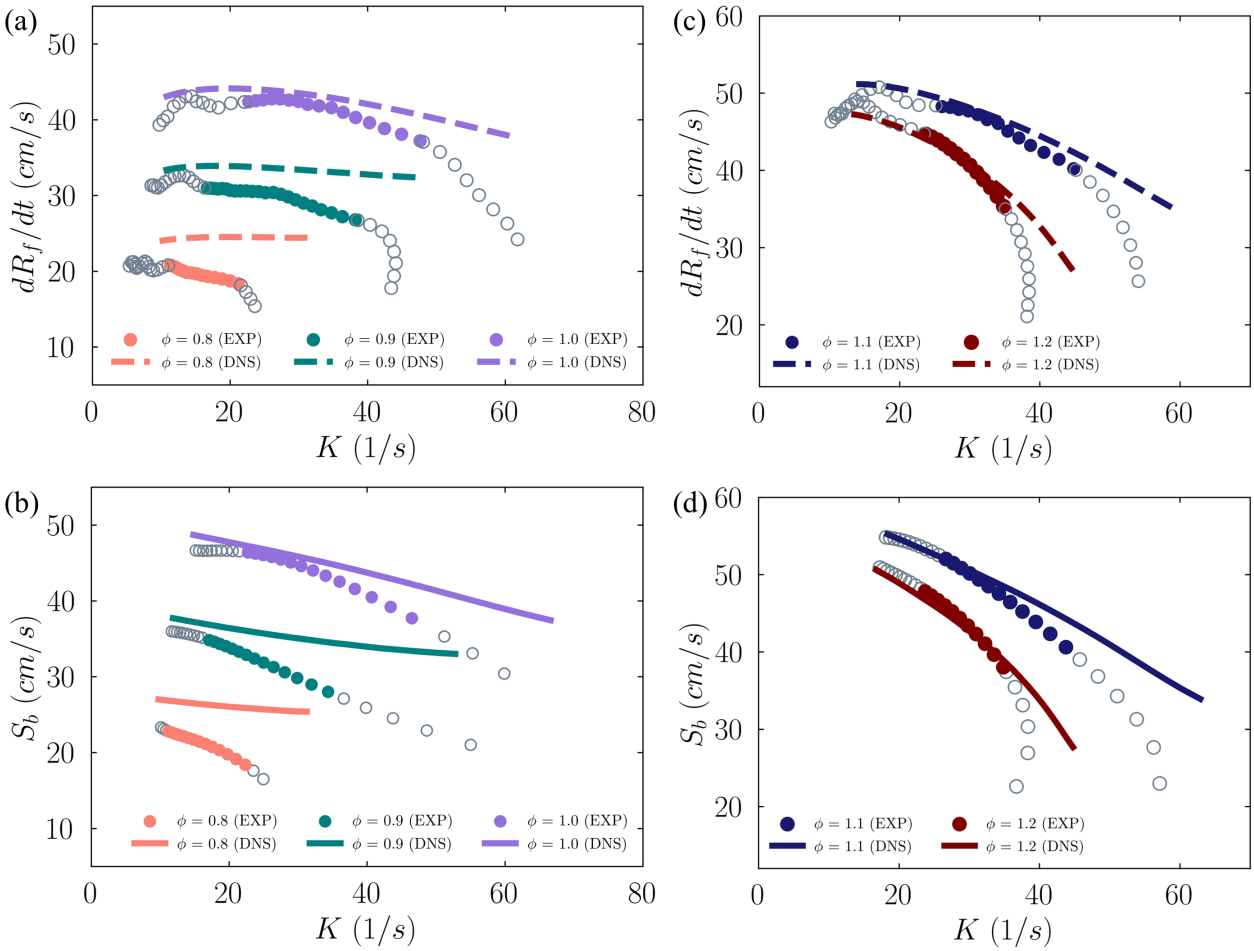

Figure 8: a) & b) Evolution of dR_f/dt from free fall experiments and OTL DNS as a function of flame stretch (solid symbols denotes data useable for extrapolation) for NH_3/air flames: $0.8 \leq \phi \leq 1.2$, P = 1 atm, and T_u = 300 K c) & d) S_b from experiments (SRADIF-corrected) and OTL DNS (DNS-corrected) (solid symbols denotes data useable for extrapolation) for NH_3/air flames: $0.8 \leq \phi \leq 1.2$, P = 1 atm, and T_u = 300 K

Figure 8a and 8b depicts dR_f/dt obtained from free fall experiments for $0.8 \leq \phi \leq 1.2$ as a function of K. Figure 8c and 8d depicts S_b that was derived by subtracting SRADIF-estimated u_b values from these dR_f/dt. Also shown in the plots are dR_f/dt with radiation heat loss (Figs. 8a and 8b) and S_b extracted from the DNS results (Figs. 8c and 8d). The full field results were utilized to calculate u_b for the radiative DNS [28]. The Nakamura et al. model [78] predictions agree with experimentally measured dR_f/dt for $\phi \geq 1$. For $\phi < 1$, the slopes and magnitude of the experimental and simulated curves differ significantly, especially at larger K. The differences observed between experimental and DNS results are also similar for the S_b vs. K curves. This is expected as it was previously shown (Fig. 7) that u_b values obtained from DNS and SRADIF are consistent. Also noticeable from the data are the prolonged ignition effects. Consequently, care has to be taken in choosing the range of R_f that will be used for extrapolation. The minimum value of R_f considered is about 7 flame thicknesses which, as a result of the large δ_f of NH_3/air flames, comes to ~1.7 cm (see Table 1). The maximum value of R_f chosen is ~3.8 cm, which is governed by the dimensions of the combustion chamber. In DNS, the flames reach quasi-steady propagation faster than what is observed in experiments, but this does not explain the large difference in magnitude and slope of these curves for the $\phi < 1$ mixtures. Most notably, the ϕ = 0.8 and ϕ = 0.9 cases show large differences in flame dynamics between experiments and computations (see Fig. 8a).

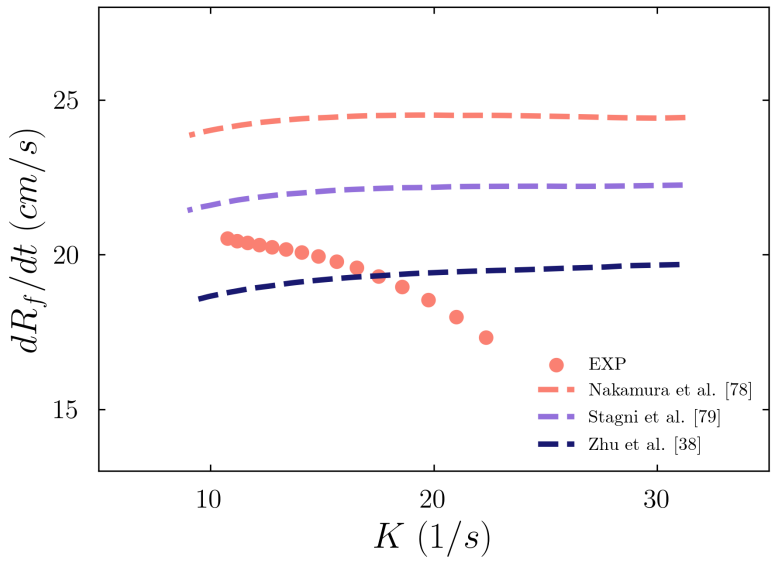

Figure 9: Comparison of experimentally measured and DNS computed dR_f/dt as a function of flame stretch using the models of Nakamura et al. [78], Stagni et al. [79], and Zhu et al. [38] for a lean NH_3/air flame (ϕ = 0.8, P = 1 atm, T_u = 300 K)

To evaluate if this observed discrepancy is due to the particular choice of kinetic model, Figure 9 compares the dR_f/dt from the ϕ = 0.8 case to predictions of three kinetic models. It is evident that all three models fail to reproduce the slope and/or magnitude of the experimental data. Furthermore, there are significant differences between the three models, which is a testament to the large uncertainty in the kinetic models for NH_3 combustion. Another reason for the observed discrepancy in slopes could be due to the assumption made in the computations that radiation reabsorption is negligible in these flames. Including radiation reabsorption would result in lower radiative heat loss and to a small extent, preheating of NH_3 in the unburned gas as was seen in the study by Zheng et al. [25] in planar NH_3/H_2/air flames. Incorporating this into the flame simulations could result in better agreement in the slope between the DNS computed and experimentally measured dR_f/dt as a function of flame stretch. This is however outside the scope of the current study and will be investigated as part of a future study. Additional comparisons, at the other equivalence ratios, with the three models considered in this study are included in SM-G.

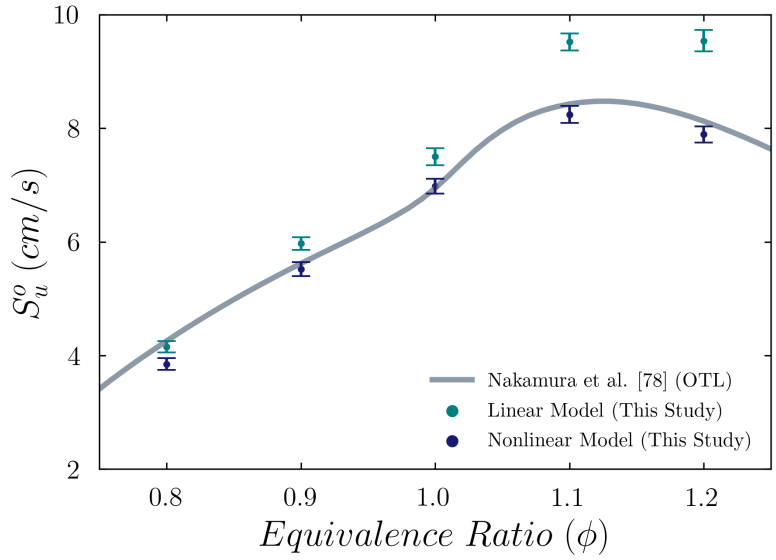

Figure 10: Experimentally derived S_u^0 using analytically derived linear and nonlinear extrapolation methods against 1-D OTL Cantera free-flame computations.

Figure 10 depicts S_u^0s derived by extrapolating the (SRADIF-corrected) S_b data using the analytically derived linear (Eqn. 3) and nonlinear models (Eqn. 4). The DNS-assisted extrapolation approach [62], which has been shown to perform well for hydrocarbon-fueled flames, was not utilized due to the significant differences in slopes between the data and model predictions observed in Fig. 8. Also plotted in Fig. 10 are results from freely propagating flame simulations using the Nakamura et al. model [78], including OTL radiation heat loss. Although the differences between the results obtained using the two extrapolation models are small for $\phi \leq 1.0$, the differences are larger on the fuel-rich side ($\phi > 1$). Prior studies [53, 54] have used the linear extrapolation model by arguing that the Lewis number (Le) is nearly unity across all ϕs for NH_3/air flames. They cite a DNS study by Chen [84] who showed good agreement between the linear and nonlinear extrapolation models for mixtures with unity Le. However, it is clearly seen in Fig. 8b that the shape of S_b vs. K curves are nonlinear, and consequently using the linear model results in systematically larger values of S_u^0 (see SM-F).

Another interesting observation from Fig. 10 is the relatively good agreement between the experimental data (derived using non-linear extrapolation) and model predictions. However, in Fig. 8, the model predictions using DNS agree with direct measurements (dR_f/dt) only for $\phi \geq 1$. For $\phi < 1$, the DNS predictions and data display significantly different slopes. Therefore, the agreement seen between the data and the model prediction in Fig. 10 for $\phi < 1$ does not necessarily mean that the model is able to reproduce the experimental data. Either the assumptions utilized for simulations and/or the extrapolation procedure utilized may not be entirely applicable under these conditions. A detailed study into the effect of radiation reabsorption on these flames could help shed light on this observed inconsistency. In any case, as mentioned in Sec. 3.2.2., comparing direct measurements with the corresponding simulations will avoid potential errors that may arise from extrapolation approaches [61]. However, this is not always feasible for fuels with complex kinetics and hence large kinetic models. Therefore, an accurate methodology is necessary to extract S_u^0 from expansion rate measurements.

The measurements made (non-linear model) are also compared with existing measurements from the literature [12, 43, 52, 53, 57] in SM-G. It is observed that other measurements are consistently lower than our measurements. Even the measurements of Han et al. [43], which uses the heat-flux approach, claim

negligible effect of buoyancy-induced flows are consistently lower than our data (> 20%). Despite the decreased confidence in our data for $\phi < 1$ (due to the inconsistency observed between Figs. 8 and 10), our measurements have carefully accounted for several aspects that introduce large errors in the derived S_u^0. Specifically, we have accounted for adsorption of NH_3 on to the chamber walls, minimized buoyancy-induced flows using a drop tower, corrected for radiation-induced flows using the SRADIF model, and evaluated the correctness of the extrapolation-approaches using DNS. Therefore, these measurements of NH_3/air S_u^0s are the most accurate to date.

5. Conclusions

In the present study, a combined experimental and computational methodology to investigate and accurately quantify the propagation rates of slow flames is presented. Slowly propagating flames are subject to gravity-induced convection and radiation heat loss, which if unaccounted for can result in incorrect interpretations of the data, and consequently large errors in measured laminar flame speeds ($S_u^0 s$). A lab-scale drop tower is developed and utilized to mitigate buoyancy-induced flows, and measure expansion rates (dR_f/dt) of slow spherically expanding flames in free fall. A computational model (SRADIF) that combines thermodynamic equilibrium and finite rate optically thin limit radiation heat loss calculations is used to estimate the radiation-induced inward flow. This inward flow velocity is subtracted from the measured dR_f/dt to obtain the flame speed relative to the burned gas (S_b), from which S_u^0 is derived. The methodology was applied first to a slowly propagating fuel-lean CH_4/air flame at 2 atm, and then to NH_3/air flames over a range of ϕ ($0.8 \leq \phi \leq 1.2$). Measurements were obtained both under static and free fall conditions to assess the errors that can arise when deriving flame speeds from natural-convection-distorted flames. The errors that can arise during the various steps of data interpretation (correction of radiation-induced flow, subtraction of stretch effects, etc.) were also analyzed. Listed below are the observations and conclusions made in this study.

1. To achieve intended NH_3/air mixture compositions, it was necessary to wait long durations (~ 1 hour) during mixture preparation to account for NH_3 adsorption on stainless steel; similar observations were previously made and discussed by others [52, 59, 63].
2. The low-cost drop tower experiment with deviations of less than 2% from the acceleration due to the earth's gravity was able to successfully establish spherical slowly propagating flames with measured dR_f/dt as low as ~20 cm/s, with a high degree of repeatability.
3. Interpreting data from buoyancy-distorted flames can result in significantly different dR_f/dt vs. stretch (K) behavior. Specifically, if the maximum horizontal dimension of the flame (as used in many previous studies) is used as a surrogate for the diameter of the buoyant, non-spherical flame, the measured dR_f/dt is consistently higher than what is derived from free fall experiments. Utilizing these incorrect measurements can result in significant errors, ~40% for the ϕ = 0.8 NH_3/air case. This demonstrates the necessity of performing free fall experiments to accurately measure slowly propagating flame speeds.
4. Analysis revealed that radiation-induced flow velocities can be significant relative to dR_f/dt for slowly propagating flames and hence needs to be subtracted from dR_f/dt to obtain S_b. The SRADIF model, which utilizes an optically thin limit radiation heat loss model, was used to estimate the inward flow velocities.
5. A systematic approach of comparing direct measurements (dR_f/dt) and derived quantities (S_b and S_u^0) to the corresponding model predictions revealed the errors that result from the post-processing steps such as correcting for radiation-induced flow and subtraction of stretch effects using extrapolation approaches. The two errors are coupled; if there radiation-induced flow is not accounted for, there will be large extrapolation errors irrespective of the extrapolation model utilized. For example, linearly extrapolating the ϕ = 0.8 NH_3/air dR_f/dt values without subtracting

radiation-induced flow velocities result in a value of S_b^0 about 20% lower than the value obtained post-correction (extrapolating S_b values). And, regarding errors that can arise from stretch correction, for ϕ = 1.2, S_b^0 values obtained by linear and non-linear extrapolation of S_b values differ by 19%.

6. For the CH_4/air case, the S_u^0 measured using the abovementioned methodology showed significant differences (~16% greater) from previous measurements which did not include effects of buoyancy-induced flow and radiation heat loss. Furthermore, the data also differed from state-of-the-art model predictions by ~22%. CH_4 is the most studied fuel in combustion; however, our results indicate that there remain modeling issues, particularly at low flame temperatures where there is strong competition between the chain branching and chain termination reactions.
7. For $\phi \geq 1.0$ NH_3/air flames, consistency was observed when comparing direct measurements (dR_f/dt) and derived S_u^0 to corresponding model predictions. However, for $\phi < 1.0$, the difference between dR_f/dt and model predictions were greater than the difference between extracted S_u^0 and model predictions. This inconsistency could mean that the extrapolation approach utilized and/or the assumptions utilized (particularly the optically thin limit model for radiation heat loss) are not entirely correct at these conditions. In any case, these results highlight the importance of comparing measurements to direct numerical simulations to assess the performance of a kinetic model.

Nevertheless, we report the most accurate measurements of NH_3/air flame speeds to date by accounting for the various physics that affect these slowly propagating flames.

6. Acknowledgements

This research was funded by the National Science Foundation (NSF) [CBET-2053239]. The authors would like to thank Behlol Nawaz, MdNayer Nasim, and Hunter Mack from the University of Massachusetts at Lowell for insightful discussions and their valuable inputs on the experimental approach and ammonia safety.

7. References

[1] C.K. Law, G.M. Faeth, Prog. Energy Combust. Sci. 20 (1994) 65-113.
[2] P.D. Ronney, Proc. Combust. Inst. 27 (1998) 2485-2506.
[3] Z. Chen, Effects of radiation and compression on propagating spherical flames of methane/air mixtures near the lean flammability limit, Combust. Flame 157 (2010) 2267-2276.
[4] G.E. Andrews, D. Bradley, Combust. Flame 18 (1972) 133-153.
[5] C.K. Wu, C.K. Law, On the determination of laminar flame speeds from stretched flames, Proc. Combust. Inst. 20 (1985) 1941-1949.
[6] F.N. Egolfopoulos, N. Hansen, Y. Ju, K. Kohse-Höinghaus, C.K. Law, F. Qi, Advances and challenges in laminar flame experiments and implications for combustion chemistry, Prog. Energy Combust. Sci. 43 (2014) 36-67.
[7] H. Wang, D.A. Sheen, Combustion kinetic model uncertainty quantification, propagation and minimization, Prog. Energy Combust. 47 (2015) 1-31.
[8] M.O. McLinden, J.S. Brown, R. Brignoli, A.F. Kazakov, P.A. Domanski, Limited options for low-global-warming-potential refrigerants, Nat. Commun. 8 (2017) 1-9.

[9] L. Berger, R. Hesse, K. Kleinheinz, M.J. Hegetschweiler, A. Attili, J. Beeckmann, G.T. Linteris, H. Pitsch, A DNS study of the impact of gravity on spherically expanding laminar premixed flames, Combust. Flame 216 (2020) 412-425.
[10] C. Bariki, F. Halter, R. Hesse, C. Chauveau, H. Pitsch, J. Beeckmann, Experimental measurements of laminar flame speeds for highly N2-diluted ethanol flames under microgravity conditions, Proc. Combust. Inst. 39 (2023) 3929-3938.
[11] R. Hesse, C. Bariki, M.J. Hegetschweiler, G.T. Linteris, H. Pitsch, J. Beeckmann, Elucidating the challenges in extracting ultra-slow flame speeds in a closed vessel-A CH2F2 microgravity case study using optical and pressure-rise data, Proc. Combust. Inst. (2022), doi:10.1016/j.proci.2022.07.167.
[12] P.D. Ronney, Effect of chemistry and transport properties on near-limit flames at microgravity, Combust. Sci. Technol. 59 (1988) 123-141.
[13] L. Qiao, Y. Gan, T. Nishiie, W.J.A. Dahm, E.S. Oran, Extinction of premixed methane/air flames in microgravity by diluents: Effects of radiation and Lewis number, Combust. Flame 157 (8) (2010) 1446-1455.
[14] H. Zhang, F.N. Egolfopoulos, Proc. Combust. Inst. 28 (2000) 1875-1882.
[15] K. Maruta, M. Yoshida, Y. Ju, T. Niioka, Proc. Combust. Inst. 26 (1996) 1283-1289.
[16] S. Wang, H. Zhang, J. Jarosinski, A. Gorczakowski, J. Podfilipski, Laminar burning velocities and Markstein lengths of premixed methane/air flames near the lean flammability limit in microgravity, Combust. Flame 157 (2010) 667-675.
[17] K. Takizawa, S. Takagi, K. Tokuhashi, S. Kondo, M. Mamiya, H. Nagai, Assessment of burning velocity test methods for mildly flammable refrigerants, Part 1: Closed-vessel method, ASHRAE Transactions 119 (2) (2013) 243-254.
[18] S.H. Sohrab, C.K. Law, Extinctions of premixed flames by stretch and radiative loss, Int. J. Heat Mass Transf. 27 (2) (1984) 291-300.
[19] Y. Ju, H. Guo, K. Maruta, F. Liu, On the extinction limit and flammability limit of non-adiabatic stretched methane–air premixed flames, J. Fluid Mech. 342 (1997) 315-334.
[20] J. Jayachandran, R. Zhao, F.N. Egolfopoulos, Determination of laminar flame speeds using stagnation and spherically expanding flames: Molecular transport and radiation effects, Combust. Flame 161 (2014) 2305-2316.
[21] J. Santner, F.M. Haas, Y. Ju, F.L. Dryer, Uncertainties in interpretation of high pressure spherical flame propagation rates due to thermal radiation, Combust. Flame 161 (2014) 147-153.
[22] H. Nakamura, M. Shindo, Effects of radiation heat loss on laminar premixed ammonia/air flames, Proc. Combust. Inst. 37 (2019) 1741-1748.
[23] M.J. Hegetschweiler, J. Pagliaro, L. Berger, R. Hesse, J. Beeckmann, H. Pitsch, G. Linteris, Effects of stretch and radiation on the laminar burning velocity of R-32/air flames, Sci. Technol. Built Environ. 26(5) (2020) 599-609.
[24] R. Hesse, L. Berger, C. Bariki, M.J Hegetschweiler, G.T Linteris, H. Pitsch, J. Beeckmann, Low global-warming-potential refrigerant CH2F2 (R-32): Integration of a radiation heat loss correction method to accurately determine experimental flame speed metrics, Proc. Combust. Inst. 38 (3) (2021) 4665–4672.
[25] S. Zheng, H. Liu, R. Sui, B. Zhou, Q. Lu, Effects of radiation reabsorption on laminar NH3/H2/air flames, Combust. Flame 235 (2022) 111699.

[26] M.J. Hegetschweiler, J.L. Pagliaro, L. Berger, R. Hesse, J. Beeckmann, C. Bariki, H. Pitsch, G.T. Linteris, Data reduction considerations for spherical R-32(CH2F2)-air flame experiments, Combust. Flame 237 (2022) 111806.
[27] M. Faghih, A. Valera-Medina, Z. Chen, A. Paykani, Effect of radiation on laminar flame speed determination in spherically propagating NH3-air, NH3/CH4-air and NH3/H2-air flames at normal temperature and pressure, Combust. Flame 257 (2023) 113030.
[28] J.K. Tavares, V. Gururajan, J. Jayachandran, Effects of radiation heat loss on planar and spherical hydrofluorocarbon/air flames, Combust. Flame 258 (2023) 113067.
[29] C.K. Law, F.N. Egolfopoulos, A unified chain-thermal theory of fundamental flammability limits, Symp. (Int.) Combust. 24(1) (1992) 137-144.
[30] H. Yu, W. Han, J. Santner, X. Gou, C.H. Sohn, Y. Ju, Z. Chen, Radiation-induced uncertainty in laminar flame speed measured from propagating spherical flames, Combust. Flame 161 (2014) 2815-2824.
[31] J. Witte, Power to Ammonia, Feasibility Study for the Value Chains and Business Cases to Produce CO2 -Free Ammonia Suitable for Various Market Applications, Institute for Sustainable Process Technology (ISPT), Amersfoort, The Netherlands, 2017 Report no. TESI115001.
[32] J.S. Cardoso, V. Silva, R.C. Rocha, M.J. Hall, M. Costa, D. Eusébio, Ammonia as an energy vector: current and future prospects for low-carbon fuel applications in internal combustion engines, J. Cleaner Prod. 296 (2021) 126562.
[33] F.J. Verkamp, M.C. Hardin, J.R. Williams, Ammonia combustion properties and performance in gas-turbine burners, Symp. (Int.) Combust. 11 (1967) 985-992.
[34] A. Valera-Medina, F. Amer-Hatem, A. Azad, I. Dedoussi, M. De Joannon, R. Fernandes, P. Glarborg, H. Hashemi, X. He, S. Mashruk, Review on ammonia as a potential fuel: from synthesis to economics, Energy Fuels 35 (2021) 6964-7029.
[35] H. Kobayashi, A. Hayakawa, K.D.K.A. Somarathne, E.C. Okafor, Science and technology of ammonia combustion, Proc. Combust. Inst. 37 (2019) 109-133.
[36] C. Dennis, B. Bojko, On the combustion of heterogeneous AP/HTPB composite propellants: a review, Fuel 254 (2019), 115646.
[37] W. Cai, P. Thakre, V. Yang, A model of AP/HTPB composite propellant combustion in rocket-motor environments, Combus. Sci. Technol. 180 (2008) 2143-2169.
[38] Y. Zhu, H.J. Curran, S. Girhe, Y. Murakami, H. Pitsch, K. Senecal, L. Yang, C. Zhou, The combustion chemistry of ammonia and ammonia/hydrogen mixtures: a comprehensive chemical kinetic modeling study, Combust. Flame 267 (2024) 113239.
[39] M. Figueroa-Labastida, L. Zheng, J.W. Streicher, R.K. Hanson, High-temperature laminar flame speed measurements of ammonia/methane blends behind reflected shock waves, Combust. Flame 261 (2024) 113314.
[40] S. Zitouni, P. Brequigny, C. Mounaïm-Rousselle, Influence of hydrogen and methane addition in laminar ammonia premixed flame on burning velocity, Lewis number and Markstein length, Combust. Flame 253 (2023) 112786.
[41] M. Kohansal, M. Kiani, S. Masoumi, S. Nourinejad, M. Ashjaee, E. Houshfar, Experimental and Numerical Investigation of NH3/CH4 Mixture Combustion Properties under Elevated Initial Pressure and Temperature, Energy Fuels 37 (2023) 10681-10696.
[42] E.C. Okafor, Y. Naito, S. Colson, A. Ichikawa, T. Kudo, A. Hayakawa, H. Kobayashi, Experimental and numerical study of the laminar burning velocity of CH4–NH3–air premixed flames, Combust. Flame 187 (2018) 185-198.

[43] X. Han, Z. Wang, M. Costa, Z. Sun, Y. He, K. Cen, Experimental and kinetic modeling study of laminar burning velocities of NH3/air, NH3/H2/air, NH3/CO/ air and NH3/CH4/air premixed flames, Combust. Flame 206 (2019) 214-226.
[44] P. Berwal, S.Kumar Shawnam, Laminar burning velocity measurement of CH4/H2/ NH3-air premixed flames at high mixture temperatures, Fuel 331 (2023) 125809.
[45] G.P. Smith, D.M. Golden, M. Frenklach, N.W. Moriarty, B. Eiteneer, M. Goldenberg, C.T. Bowman, R.K. Hanson, S. Song, W. Gardiner Jr, GRI-Mech 3.0, 1999, combustion.berkeley.edu/gri_mech, (2011).
[46] E.C. Okafor, Y. Naito , S. Colson , A. Ichikawa , T. Kudo , A. Hayakawa , H. Kobayashi , Experimental and numerical study of the laminar burning velocity of CH 4 –NH 3 –air premixed flames, Combust. Flame 187 (2018) 185-198.
[47] U. Mechanism, Chemical-kinetic mechanisms for combustion applications, mechanical and aerospace engineering (combustion research), University of California at San Diego, 2014 . http://web.eng.ucsd.edu/mae/groups/combustion/ mechanism.html.
[48] J. Otomo, M. Koshi, T. Mitsumori, H. Iwasaki, K. Yamada, Chemical kinetic modeling of ammonia oxidation with improved reaction mechanism for ammonia/air and ammonia/hydrogen/air combustion, Int. J. Hydrog. Energy 43 (5) (2018) 3004-3014.
[49] T. Jabbour, D.F. Clodic , J. Terry , S. Kondo , Burning velocity and refrigerant flammability classification, ASHRAE Trans. 110 (2004) 522-533.
[50] U. Pfahl, M. Ross , J. Shepherd , K. Pasamehmetoglu , C. Unal , Flammability limits, ignition energy, and flame speeds in H2–CH4–NH3–N2O–O2–N2 mixtures, Combust. Flame 123 (2000) 140-158.
[51] V.F. Zakaznov, L.A. Kursheva, Z.I. Fedina, Determination of normal flame velocity and critical diameter of flame extinction in ammonia-air mixture, Combust. Explos. 14 (1978) 710-713.
[52] K. Takizawa, A. Takahashi, K. Tokuhashi, S. Kondo, A. Sekiya, Burning velocity measurements of nitrogen-containing compounds, J. Hazard. Mater. 155 (2008) 144-152.
[53] A. Hayakawa, T. Goto , R. Mimoto , Y. Arakawa , T. Kudo , H. Kobayashi , Laminar burning velocity and Markstein length of ammonia/air premixed flames at various pressures, Fuel 159 (2015) 98-106.
[54] A . Ichikawa, A . Hayakawa , Y. Kitagawa , K.D.K.A. Somarathne , T. Kudo , H. Kobayashi , Laminar burning velocity and Markstein length of ammonia/hydrogen/air premixed flames at elevated pressures, Int. J. Hydrog. Energy 40 (2015) 9570-9578.
[55] Y. Li, M. Bi, B. Li, W. Gao, Explosion behaviors of ammonia–air mixtures, Combust. Sci. Technol. 190 (2018) 1804-1816.
[56] B. Mei, X. Zhang , S. Ma , M. Cui , H. Guo , Z. Cao , Y. Li , Experimental and kinetic modeling investigation on the laminar flame propagation of ammonia under oxygen enrichment and elevated pressure conditions, Combust. Flame 210 (2019) 236-246.
[57] C. Lhuillier, P. Brequigny , N. Lamoureux , F. Contino , C. Mounaïm-Rousselle , Experimental investigation on laminar burning velocities of ammonia/hydrogen/air mixtures at elevated temperatures, Fuel 263 (2020) 116653.
[58] X. Chen, Q. Liu, Q. Jing, Z. Mou, Y. Shen, J. Huang, H. Ma, Flame front evolution and laminar flame parameter evaluation of buoyancy-affected ammonia/air flames, Int. J. Hydrogen Energy 46 (2021) 38504-38518.
[59] L.F. Alvarez, J. Shaffer, C.E. Dumitrescu, O. Askari, Laminar burning velocity of Ammonia/Air mixtures at high pressures, Fuel 363 (2024) 130986.

[60] R. Kanoshima, A. Hayakawa, T. Kudo, E.C. Okafor, S. Colson, A. Ichikawa, T. Kudo, H. Kobayashi, Effects of initial mixture temperature and pressure on laminar burning velocity and Markstein length of ammonia/air premixed laminar flames, Fuel 310 (2022) 122149.
[61] J. Jayachandran, A. Lefebvre, R. Zhao, F. Halter, E. Varea, B. Renou, F.N. Egolfopoulos, A study of propagation of spherically expanding and counterflow laminar flames using direct measurements and numerical simulations, Proc. Combust. Inst. 35 (2015) 695–702.
[62] C. Xiouris, T. Ye, J. Jayachandran, F.N. Egolfopoulos, Laminar flame speeds under enginerelevant conditions: Uncertainty quantification and minimization in spherically expanding flame experiments, Combust. Flame 163 (2016) 270-283.
[63] O. Mathieu, E.L. Petersen, Experimental and modeling study on the high-temperature oxidation of ammonia and related NOx chemistry, Combust. Flame 162 (2015) 554-570..
[64] F. Halter, Z. Chen, G. Dayma, C. Bariki, Y. Wang, P. Dagaut, C. Chauveau, Development of an optically accessible apparatus to characterize the evolution of spherically expanding flames under constant volume conditions, Combust. Flame 212 (2020) 165-176.
[65] G. Taubin, Estimation Of Planar Curves, Surfaces And Nonplanar Space Curves Defined By Implicit Equations, With Applications To Edge And Range Image Segmentation, IEEE Trans. PAMI 13 (1991) 1115-1138.
[66] D.R. Dowdy, D.B. Smith, S.C. Taylor, A. Williams, The use of expanding spherical flames to determine burning velocities and stretch effects in hydrogen/air mixtures, Proc. Combust. Inst. 23 (1990) 325-332.
[67] P. Clavin, Dynamic behavior of premixed flame fronts in laminar and turbulent flows, Prog. Energy Combust. Sci. 11 (1985) 1-59.
[68] P. Ronney, G. Sivashinsky, A theoretical study of propagation and extinction of nonsteady spherical flame fronts, SIAM J. Appl. Math. 49 (4) (1989) 1029-1046.
[69] A.P. Kelley, C. Law, Nonlinear effects in the extraction of laminar flame speeds from expanding spherical flames, Combust. Flame 156 (9) (2009) 1844-1851.
[70] Z. Chen, M.P. Burke, Y. Ju, Effects of compression and stretch on the determination of laminar flame speeds using propagating spherical flames, Combust. Theory Model. 13 (2009) 343-364.
[71] M.P. Burke, Z. Chen, Y. Ju, F.L. Dryer, Effect of cylindrical confinement on the determination of laminar flame speeds using outwardly propagating flames, Combust. Flame 156 (2009) 771–779.
[72] Z. Chen, M.P. Burke, Y. Ju, Effects of Lewis number and ignition energy on the determination of laminar flame speed using propagating spherical flames, Proc. Combust. Inst. 32 (2009) 1253–1260.
[73] Z. Chen, M.P. Burke, Y. Ju, On the critical flame radius and minimum ignition energy for spherical flame initiation, Proc. Combust. Inst. 33 (2011) 1219–1226.
[74] A.P. Kelley, G. Jomaas, C.K. Law, Critical radius for sustained propagation of spark-ignited spherical flames, Combust. Flame 156 (2009) 1006–1013.
[75] D.G. Goodwin, R.L. Speth, H.K. Moffat, B.W. Weber, Cantera: An object-oriented software toolkit for chemical kinetics, thermodynamics, and transport processes. https://www.cantera.org , 2021. Version 2.5.0.
[76] D.R. Burgess Jr., R.R. Burrell, V.I. Babushok, J.A. Manion, M.J. Hegetschweiler, G.T. Linteris, Burning velocities of R-32/O2/N2 mixtures: Experimental measurements and development of a validated detailed chemical kinetic model, Combust. Flame 236 (2022).

[77] G.P. Smith, Y. Tao, H. Wang, Foundational Fuel Chemistry Model Version 1.0 (FFCM-1), http://nanoenergy.stanford.edu/ffcm1, 2016.
[78] H. Nakamura, et al., Kinetic modeling of ammonia/air weak flames in a micro flow reactor with a controlled temperature profile, Combust. Flame 185 (2017) 16-27.
[79] A. Stagni, et al., An experimental, theoretical and kinetic-modeling study of the gas-phase oxidation of ammonia, React. Chem. Eng. 5 (2020) 696-711.
[80] R.S. Barlow, A.N. Karpetis, J.H. Frank, J.Y. Chen, Scalar profiles and NO formation in laminar opposed-flow partially premixed methane/air flames, Combust. Flame 127(3) (2001) 2102-2118.
[81] M.I. Hassan, K.T. Aung, G.M. Faeth, Measured and predicted properties of laminar premixed methane/air flames at various pressures, Combust. Flame 115 (1998) 539-550.
[82] G. Rozenchan, D.L. Zhu, C.K. Law, S.D. Tse, Outward propagation, burning velocities, and chemical effects of methane flames up to 60 atm, Proc. Combust. Inst. 29 (2002) 1461-1470.
[83] D.L. Zhu, F.N. Egolfopoulos, C.K. Law, Experimental and numerical determination of laminar flame speeds of methane/(Ar, N2, CO2)-air mixtures as function of stoichiometry, pressure, and flame temperature, Symp. Combust. 22 (1989) 1537-1545.
[84] Z. Chen, On the extraction of laminar flame speed and Markstein length from outwardly propagating spherical flames, Combust. Flame 158 (2011) 291-300.